Supplementary Information

S1 List of institutions involved in EMeRGe

Project Partners			
Institution	**Head of Department**	**Principal Investigator**	**Link**
University of Bremen Institute of Environmental Physics: - Physics and Chemistry of the Atmosphere	Prof. Dr. John P. Burrows	Prof. Dr. John P. Burrows / Dr. Maria Dolores Andrés Hernández	www.iup.uni-bremen.de
University of Bremen LAMOS - Laboratory for Modeling and Observation of the Earth System	Prof. Dr. Mihalis Vrekoussis	Prof. Dr. Mihalis Vrekoussis / (in cooperation with Dr. Andrea Pozzer_MPI)	www.iup.uni-bremen.de/lamos
DLR - German Aerospace Center Institute of Atmospheric Physics	Prof. Dr. Markus Rapp	Dr. Hans Schlager / Dr. Helmut Ziereis / Dr. Daniel Sauer	www.dlr.de/pa
Max Planck Institute for Chemistry Particle Chemistry	Prof. Dr. Stephan Borrmann	Dr. Johannes Schneider	www.mpic.de/
Max-Planck-Institute for Chemistry Multiphase Chemistry	Prof. Dr. Ulrich Pöschl	Dr. Mira Pöhlker	www.mpic.de
Johannes Gutenberg University Mainz Institute for Atmospheric Physics: - Aerosol and Cloud Physics	Prof. Dr. Stephan Borrmann	Prof. Dr. Stephan Borrmann	www.ipa.uni-mainz.de
Heidelberg University Institute of Environmental Physics: - Tropospheric Chemistry	Prof. Dr. Ulrich Platt	Prof. Dr. Ulrich Platt / Dr. Denis Pöhler	www.iup.uni-heidelberg.de
Heidelberg University Institute of Environmental Physics: - Atmospheric Radiation and Applications	Prof. Dr. Klaus Pfeilsticker	Prof. Dr. Klaus Pfeilsticker	www.iup.uni-heidelberg.de/
University of Wuppertal Institute for Atmospheric and Environmental Research	Prof. Dr. Ralf Koppmann	Prof. Dr. Ralf Koppmann / Dr. Marc Krebsbach	www.iau.uni-wuppertal.de
Karlsruhe Institute of Technology (KIT) Institute of Meteorology and Climate Research: - Atmospheric Trace Gases and Remote Sensing	Prof. Dr. Peter Braesicke	Dr. Andreas Zahn / Dr. Harald Bönisch	www.imk-asf.kit.edu
Forschungszentrum Jülich Institute of Energy and Climate Research: Troposphere (IEK-8)	Prof. Dr. Astrid Kiendler-Scharr / Prof. Dr. Andreas Wahner	Dr. Birger Bohn	www.fz-juelich.de/iek/iek-8

5 **S2 List of institutions involved in EMeRGe international**

European Partners		
Country	**Institution**	**Link**
Belgium	**KMI** - Royal Meteorological Institute of Belgium	www.meteo.be
France	**CNRS** - French National Centre for Scientific Research	www.cnrs.fr
	University of Lille	www.univ-lille1.fr
Germany	**DWD** - German Meteorological Service - Meteorological Observatory Hohenpeissenberg - Richard Assmann Observatory Lindenberg	www.dwd.de
	IASS - Institute for Advanced Sustainability Studies	www.iass-potsdam.de www.uc2-program.org
	TROPOS - Leibniz Institute for Tropospheric Research	www.tropos.de
Greece	**Aristotle University of Thessaloniki**	www.auth.gr
	FORTH - Foundation for Research and Technology - Hellas	www.forth.gr
	IERSD - Institute for Environmental Research and Sustainable Development, National Observatory of Athens	www.iersd.noa.gr
	National Technical University Of Athens	www.ntua.gr
	NOA - National Observatory of Athens	www.noa.gr
	PANACEA - Panhellenic infrastructure for Atmospheric Composition and Climate Change	panacea-ri.gr
	University of Crete	www.uoc.gr
Ireland	**UCC** - University College of Cork	www.ucc.ie
Italy	**CNR-ISAC** - National Research Council of Italy, Institute of Atmospheric Sciences and Climate	www.isac.cnr.it
	CNR-IMAA - National Research Council of Italy **I**stituto di Metodologie per l'Analisi Ambientale	www.imaa.cnr.it
	University of L'Aquila JRC	www.univaq.it
	University of Naples Federico II	www.unina.it
	Sapienza University of Rome	www.phys.uniroma1.it
	University of Salento, Mathematics and Physics Department	www.unisalento.it
Netherlands	**KNMI** - Royal Netherlands Meteorological Institute	www.knmi.nl
Spain	**CEAM** – Mediterranean Center for Environmental Studies	www.ceam.es
	CIEMAT- Centro de Investigaciones Energéticas, Medioambientales y Tecnológicas	www.ciemat.es
	IDAEA-CSIC – Spanish National Research Council, Institute of Environmental Assessment and Water Research	www.idaea.csic.es
	University of Granada	www.ugr.es

	University of Valencia	www.uv.es
	UPC - Universitat Politècnica de Catalunya	www.upc.edu
United Kingdom	**NCAS** - National Center for Atmospheric Science	www.ncas.ac.uk
	University of Hertfordshire	www.herts.ac.uk
	University of Manchester	www.manchester.ac.uk
	University of York	www.york.ac.uk
	FAAM - Facility for Airborne Atmospheric Measurements	www.faam.ac.uk
Asian Partners		
Country	**Institution**	**Link**
Japan	**Chubu University**	www.chubu.ac.jp
	Chiba University	www.chiba-u.jp
	CRIEPI - Central Research Institute of Electric Power Industry	criepi.denken.or.jp
	Fukuoka University	www.fukuoka-u.ac.jp
	JAMSTEC - Japan Agency for Marine-Earth Science and Technology,- Research Institute for Global Change (RIGC)	www.jamstec.go.jp
	JAXA - Japan Aerospace Exploration Agency	www.jaxa.jp
	JMA - Japan Meteorological Agency	www.jma.go.jp
	Kanazawa University,Institute of Nature and Environmental Technology	www.kanazawa-u.ac.jp
	Kobe University	www.kobe-u.ac.jp
	Kyushu University	www.kyushu-u.ac.jp
	MRI - Meteorology Research Institute	www.mri-jma.go.jp
	Nagoya University	www.nagoya-u.ac.jp
	Nara Womens's University, - Department of Chemistry, Biology and Environmental Science	www.nara-wu.ac.jp
	NICT - National Institute of Information and Communications Technology	www.nict.go.jp
	NIES - National Institute for Environmental Studies	www.nies.go.jp
	NIPR - National Institute of Polar Research	www.nipr.ac.jp
	Osaka Prefecture University, - Department of Applied Chemistry	www.osakafu-u.ac.jp
	Tokyo Metropolitan University	www.tmu.ac.jp
	University of Tokyo	www.u-tokyo.ac.jp
	University of Toyama	www.u-toyama.ac.jp
Peoples's Republic of China	**Peking University,** College of Environmental Sciences and Engineering	www.pku.edu.cn
	Nanjing University, School of Atmospheric Science	www.nju.edu.cn
	Jinan University, Guangzhou	www.jnu.edu.cn

Philippines	**Oscar M. Lopez Center** for Climate Change and Disaster Management Foundation	www.omlopezcenter.org
	University of the Philippines Diliman, - IESM - Institute of Environmental Science and Meteorology	upd.edu.ph
	HUFS - Hankuk University of Foreign Studies, - Department of Environmental Science	www.hufs.ac.kr
Republic of Korea	**Seoul National University** - School of Earth and Environmental Sciences), - Atmospheric & Climate Environment Laboratory	www.snu.ac.kr
	Yonsei University Atmospheric Radiation Laboratory	www.yonsei.ac.kr
	Academia Sinica **- RCEC** - Reseach Center for Environmental Changes	www.sinica.edu.tw
Taiwan (Republic of China)	**NTU** - National Taiwan University	www.ntu.edu.tw
	NCKU – National Cheng Kung University, Tainan	www.iaa.ncku.edu.tw
	AIT - Asian Institute of Technology, - SERD - School of Environment, Resources and Development	www.ait.ac.th
Thailand	**LPRU** - Lampang Rajabhat University, - Faculty of Science, Atmospheric Science and Astronomy Research Unit	www.lpru.ac.th
	NARIT - National Astronomical Research Institute of Thailand, - Near-Earth Objects, Space Weather and Earth's Climate	www.narit.or.th
	NARIT - National Astronomical Research Institute of Thailand, - Near-Earth Objects, Space Weather and Earth's Climate	www.narit.or.th
Other Partners		
Country	**Institution**	**Link**
European Union	**JRC** - EU Science Hub - Joint Research Centre, Ispra	ec.europa.eu/jrc/en/about/ jrc-site/ispra
Australia	**UOW** - University of Wollongong, - Centre for Atmospheric Chemistry	www.uow.edu.au
United States of America	**Georgia Institute of Technology,** - Earth and Atmospheric Sciences	www.gatech.edu

S3 Model simulations used for flight planning

S3.1 CAMS

CAMS (Copernicus Atmosphere Monitoring Service, http://atmosphere.copernicus. eu) is the successor of the former GEMS (Global and regional Earth-system Monitoring using Satellite and in-situ data) (Hollingsworth et al., 2008) and three succeeding MACC (Monitoring Atmospheric Composition and Climate, http://www.gmes-atmosphere.eu/) projects. It extends weather services of the ECMWF (European Centre for Medium-Range Weather Forecasts) with simulations of atmospheric trace gases and aerosols as part of its global component. Operational air quality forecasts and analyses for Europe are provided at much finer resolution through the regional component.

CAMS-global simulations of atmospheric composition are based on the C-IFS (Composition - Integrated Forecasting System; Flemming et al., 2015) of the ECMWF. C-IFS is a version of the CB05 (Carbon Bond 2005 chemistry scheme; Huijnen et al., 2010) derived from the CTM Transport Model 5 (TM5). Within C-IFS, modules of atmospheric chemistry and physical processes are integrated on-line and several ground-based and satellite data are assimilated (see Innes et al., 2015). For EMeRGe in Europe, CO passive tracer forecasts for the MPCs of London, the Ruhr area, Amsterdam/Rotterdam, Berlin, Po Valley, Madrid, Paris, Rome and of biomass burning from Europe, North America and Siberia were provided through the CAMS field campaign support (see also Flemming et al., 2019) service. A stratospheric ozone tracer subject to loss in the troposphere from the CAMS operational model system was used as indicator of stratospheric versus tropospheric air masses. For flight planning and analysis of conditions for EMeRGe in Europe, the CAMS tracer output is used in addition to full atmospheric chemistry runs of the operational suite. The CAMS-global simulations were performed with T511L60 model resolution. The MACCity (Granier et al., 2011) emission inventory is used for anthropogenic emissions, GFASv1.2 (Kaiser et al., 2012) for near-real-time fire emissions, and a climatology of MEGAN-MACC (Sindelarova et al., 2014) for biogenic emissions. Stratospheric chemistry is not implemented in C-IFS, stratospheric ozone is derived from the Cariolle scheme (Cariolle and Teyssèdre, 2007), stratospheric NO_x is implicitly constrained by fixing the HNO_3/O_3 ratio at the 10 hPa level.

S3.2 HYSPLIT

The Lagrangian Particle Dispersion Model HYSPLIT (https://www.arl.noaa. gov/hysplit/) was used to calculate the transport and dispersion of local CO emissions, accumulated over 6 days. The values do not include accumulated "background" concentrations due to the much longer life-time of CO and are thus not to be compared with absolute concentrations but rather with "enhancements" inside of local plumes. HYSPLIT was driven by meteorology data from operational ECMWF forecast (0-11 hours forecast, 12-hourly update, interpolated at 0.1 deg horizontally, pressure levels, 1-hourly output). CO emission rates were taken from EDGAR HTAP V2 emission inventory, http://edgar.jrc.ec.europa.eu/htap_v2/). Dry and wet deposition can be modelled, but no chemical reactions. No convection, only large-scale vertical movements as provided by the meteorological data set used as input. The computation (core-model) and the visualisation (post-processing) are controlled by a specific client-server infrastructure developed at DLR-IPA for campaign-support as well as post-campaign analysis.

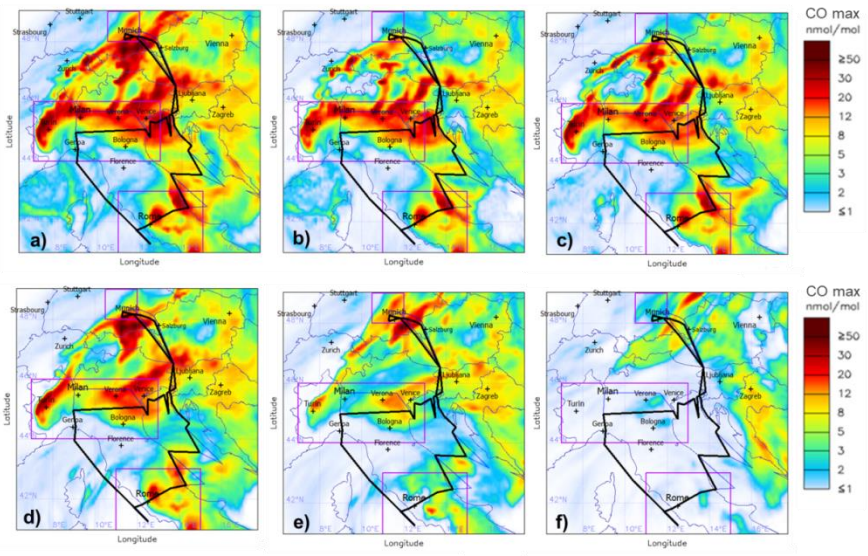

Figure S3.1. Example of HYSPLIT forecast for the flight planning on 20 July 2017 resulting from a 6 days accumulation of CO from selected EU metropolitan areas, as indicated by the squares (in purple). In this example the ECWMF forecast is initialised on 19 July 2017 at 12 UTC for a) total maximum volume mixing ratio (VMR) between ground level and 3200m, b) mean VMR between 300-700m above ground level (agl), c) mean VMR between 700-1200m agl d) mean VMR between 1200-1800m agl, e) mean VMR between 1800-2500m agl, and f) mean VMR between 2500-3200m agl; all averaged from 12 to 15 UTC. The flight track is superimposed in black.

S4 BAHAMAS

Basic meteorological and aircraft data were provided from DLR-FX developed BAHAMAS (BAsic HALO Measurement And Sensor System) instrument at 1s and 0.1s time resolution in NASA Ames and NetCDF (Network Common Data Form) format. In standard configuration BAHAMAS acquires data from airflow and thermodynamic sensors as well as from the aircraft avionics and a high-precision GNSS/IMU (Global Navigation Satellite System / Inertial Measurement Unit) system to derive basic meteorological parameters like pressure, temperature, humidity, and the 3-D wind vector as well as aircraft position and attitude.

High accuracy water vapor concentration and further derived humidity parameters are measured by SHARC (Sophisticated Hygrometer for Atmospheric ResearCh) instrument, installed inside of BAHAMAS, based on direct absorption measurement by a tunable diode laser (TDL) system.

Typical absolute accuracy of the basic meteorological data is 0.3hPa for static pressure, 0.5K for temperature, 0.5m s^{-1} for east and north and 0.3m s^{-1} for vertical wind component, 10m for pressure altitude, 4.2m for altitude above mean sea level (Schumann, 2020) and 5% ± 1ppmv for water vapor volume mixing ratio from SHARC (Schulz et al., 2018).

Table S4.1. BAHAMAS 1Hz and 10Hz standard output data.

Data	Parameter [unit]	Data	Parameter [unit]
Time	Seconds after midnight (UTC)	Meteorological	Pressure altitude [m]
Aircraft position and attitude	WGS84 altitude [m]		Calculated altitude above sea level from meteorological data [m]
	WGS84 latitude and longitude[°]		Static pressure [hPa]
	root mean square value for x-, y- and z-position [m]		Dynamic pressure [hPa]
	Ground speed [m s^{-1}]		Static air temperature [K]
	Calculated true air speed [m s^{-1}]		Total air temperature [K]
	Mach number [Ma]		Potential temperature [K]
	North-, East-, up-velocity [m s^{-1}]		Virtual temperature [K]
	x-, y- and z-axis acceleration [m s^{-2}]		Virtual potential temperature [K]
	Vertical acceleration [m s^{-2}]		Dewpoint temperature [K]
	Angle of attack [°]		Absolute humidity [g m^{-3}]
	Angle of sideslip [°]		Relative humidity respect to water [%]
	Actual track angle [°]		H_2O volume mixing ratio [μmol mol^{-1}]
	True heading [°]		H_2O mass mixing ratio [g kg^{-1}]
	Pitch angle [°]		Horizontal wind direction [°]
	Roll angle [°]		Horizontal windspeed [m s^{-1}]
	Yaw rate [° s^{-1}]		Wind vector North component [m s^{-1}]
	Pitch rate [° s^{-1}]		Wind vector East component [m s^{-1}]
	Roll rate [° s^{-1}]		Wind vector vertical component [m s^{-1}]

S5 HALO-FAAM intercomparison exercise

HALO and FAAM research aircrafts flew in close formation for 1.6 hours around noon in the northern part of a restricted airspace, "TRA Allgaeu", between Augsburg and Ulm, in Southern Germany. HALO and FAAM flew closely together in a racetrack pattern on three flight levels. The formation flight started at FL150 (4572 m) in a rather dry and clean troposphere and ended at FL 40 (1219 m) in a more polluted convective boundary layer. Table S5.1 summarises the instrumentation on- board FAAM available for comparison. In total, 24 instruments were operated on the two aircraft and provided data for the comparison.

The uploaded data were evaluated by an external referee. The data collection identified 28 parameters sampled on both aircrafts and further 13 pairs of data from sampling on either HALO or FAAM. In addition, observational data were collected from the German Weather Service at the observatory Hohenpeissenberg, located about 1000 m above sea level and 40 to 100 km downstream of the aircraft track in the TRA Allgaeu, and model results were generated from 6 models and interpolated along the common flight path. Together, the combined data set includes 221 parameters allowing for comparisons between 277 pairs of data. An overview of the measured and modelled data available for direct comparisons is provided in the following tables. More details on the intercomparison results can be found in Schumann (2020)

Table S5.1. FAAM instrumentation for the intercomparison exercise on 13 July 2017. NS: navigation system; SDPS: Static and dynamic pressure sensor; PtRT: platinum resistance thermometers; RH: relative humidity; C-ToF-AMS: Compact time-

of-flight aerosol mass spectrometer; CPC: Condensation Particle Counting; FGGA: Fast greenhouse gas analyser; TILDAS: Tunable IR laser direct absorption spectrometer; WAS-GC-FID: Whole air canister sample - Gas chromatography - Flame-ionization detection; OA.-COS: Off axis-integrated cavity output spectroscopy, AC: Academic institution

FAAM measurements			
Species/parameters	**Acronym**	**Institution**	**Technique/Instrument**
Org, NO_3, SO_4, NH_4, Chl, Org44	AMS	Manchester AC	C-ToF-AMS
NO, NO_2	AQD	York AC	Chemiluminescence
Lon, Lat, altitude , T, U, V, W, T_DI, CO, (O_3), H_2O, P, CPC, RH	CORE	FAAM	Satellite/inertial NS, SDPS, PtRT, VUV fluorometry (CO), UV photometry (O_3), CPC
CH_4, CO_2	FGGA	NERC AC	OA-COS
Np, Dp	SMPS	Manchester AC	Scanning mobility particle sizer
rBCm, rBCn, SCn, MMD, CTTR	SP2	Manchester AC	Single particle soot photometry
C_2H_6	TILDAS	Manchester AC/York AC	Laser absorption spectrometry
C_2H_6, C_2H_4, C_3H_8, C_3H_6, C_4H_{10},C_2H_2, C_5H_{10}, C_5H_{12}, C_4H_6, C_6H_{14}, C_7H_{16}, C_6H_6, C_8H_{18}, C_8H_{18},C_7H_8	WAS-GC-FID	York AC	Off line GC-FID

Table S5.2. Overview of measured and model data available for the intercomparison exercise on 13 July 2017. x, xx, xxx denotes data from 1, 2 or 3 instruments on one aircraft, and (x): outside comparison period. Columns: HALO and FAAM: aircraft instruments; HOP: measurements at Germany Weather Service (Deutscher Wetterdienst, DWD) Hohenpeissenberg; Models: CAMS: Copernicus Atmosphere Monitoring Service model, EMAC: Global ECHAM/MESSy atmospheric climate/chemistry model, MECO: Regional air chemistry/climate model based on ECHAM/COSMO, CESM2: air chemistry version of the CAM6 model, Photo: a photochemistry equilibrium model, IFS: Integrated Forecasting System (IFS) of the European Centre for Medium-Range Weather Forecasts (ECMWF).

	HALO	FAAM	HOP	CAMS	EMAC	MECO	CESM2	Box	IFS
CO_2	x	x	x		x	x			
CH_4	x	x	x	x	x	x	x		
O_3	xx		x	x	x	x	x		
CO	x	x	x	x	x	x	x		
NO	x	x	x	x	x	x	x		
NO_2	x	x	x	x	x	x	x	x	
HONO	x				x	x	x		
HNO_3	x			x	x	x	x		
PAN	(x)			x	x	x	x		
NOy	x				x	x	x		
J_{NO2}, J_{O1D}, …	x		x		x	x	x		
SO_2	x			x	x	x	x		
RO_2	x				x	x	x		
Org aerosol	x	x	x	x			x		
NO_3 aerosol	x	x	x				x		
SO_4 aerosol	x	x	x	x			x		
NH_4 aerosol	x	x	x				x		
Chl aerosol	x	x	x	x			x		
Org44 aerosol	x	x	x				x		
BCm aerosol	x	x	x	x			x		
BCn aerosol	x	x	x				x		
SCn aerosol	x	x	x				x		
CPC	x	x	x						
CH_2O_FOR	xx		x	x	x	x	x		
C_2H_6_ETA		xx	x	x	x	x	x		
CH_3OH_MET	xx		x		x	x	x		
C_2H_4O_ACA	xx		x		x	x	x		
C_3H_6O_ACE	xx		x		x	x	x		
C_5H_8_ISO	xx		x	x	x	x	x		
C_6H_6_BEN	xxx	x	x				x		
C_7H_8_TOL	xxx	x	x				x		
C_8H_{10}_XYL	xxx		x				x		
C_7H_{16}_HEP	x	x	x				x		
CCl_4	x		x		x	x			
H_2O, RH	x	x	x	x	x	x	x		x
U, V, W	x	x	x	x	x	x	x		x
T, p, h, lon, lat	x	x	x	x	x	x	x		x

S6 Ground based measurements of trace gases and aerosols

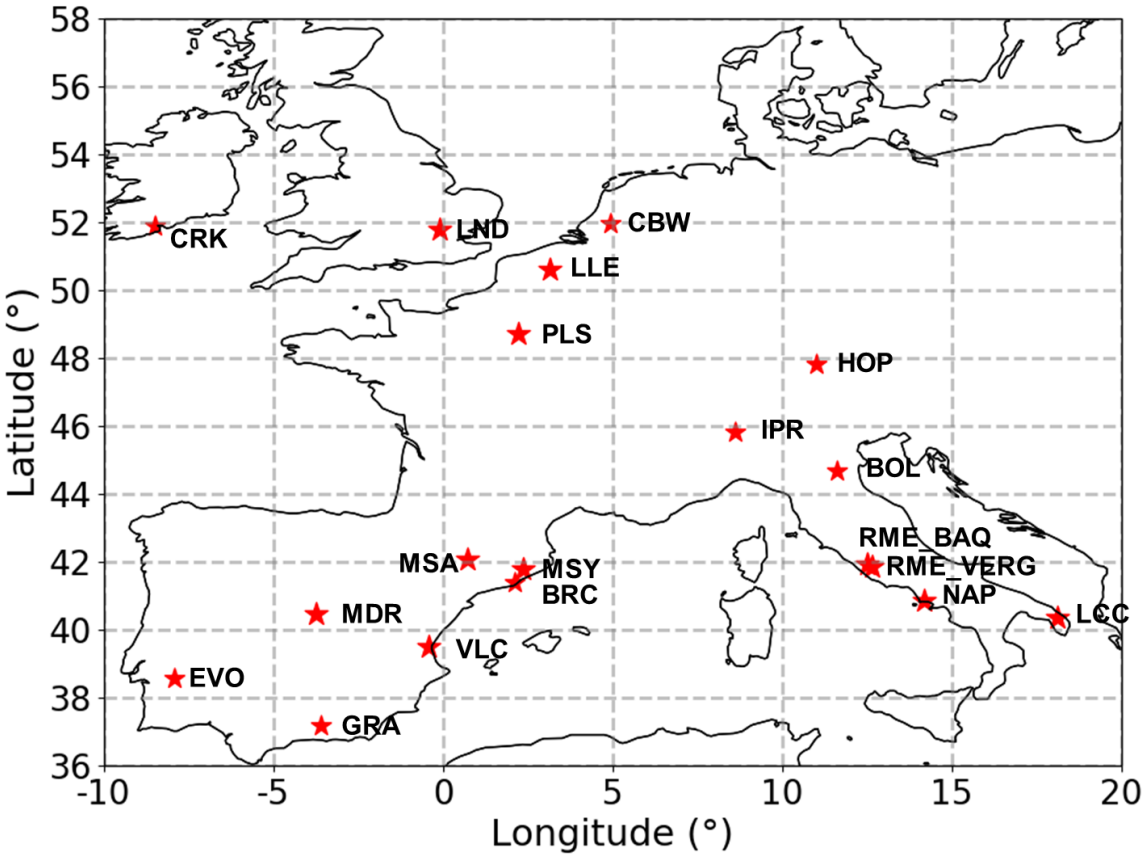

Figure S6.1. Coordinated lidar and ceilometer measurements during the EMeRGe campaign in Europe. Names corresponding to the abbreviations are listed in Table S6.1.

Table S6.1. Coordinated lidar and ceilometer measurements provided from EARLINET ground based stations during the EMeRGe IOP in Europe, Coordinates, abbreviations and principal investigators are additionally specified Multiwavelength-Polarization; MR: Multiwavelength-Raman; MPR: Multiwavelength-Polarization-Raman; PR: Polarization-Raman.

Station	Coordinates	Instrument	Principal Investigator
Barcelona (BRC)	41.386 N 2.117 E	Polarization-Lidar	J. M. Baldasano, M. Sicard
Bologna (BOL)	44.652 N 11.624 E	Polarization-Lidar	A. Marinoni
Cabauw (CBW)	51.970 N 4.930 E	MPR Lidar	A. Apituley
Cork (CRK)	51.893 N -8.494 E	PR Lidar	A. Ruth
Evora (EVO)	38.568 N -7.912 E	MPR Lidar	D. Bortoli
Granada (GRA)	37.1640 N -3.605 E	MPR Lidar	L. A. Arboledas
Hohenpeissenberg (HOP)	47.802 N 11.012 E	MPR Lidar	I. Mattis
Ispra (IPR)	45.817 N 8.617 E	MPR Lidar	J.-P. Putaud
Lecce (LCC)	40.333 N 18.100 E	Multiwavelength-Lidar	M. R. Perrone
Lille (LLE)	50.612 N 3.142E	MP Lidar	P. Goloub
London (LND)	51.775 N -0.095 E	Lidar	D. Müller
Madrid (MDR)	40.456 N -3.726 E	MR Lidar	M. Pujadas
Montsec (MSA)	42.050 N 0.733 E	Ceilometer	A. Alastuey
Montseny (MSY)	41.767 N 2.350 E	Ceilometer	A. Alastuey
Naples (NAP)	40.838 N 14.183 E	MPR Lidar	N. Spinelli
Palaiseau (PLS)	48.713 N 2.208 E	MP Lidar	M. Haeffelin
Rome I (RME_BAQ)	41.920 N 12.520 E	MPR Lidar	M. Campanelli, F. Barnaba
Rome II (RME_VERG)	41.833 N 12.650 E	Raman-Lidar	
Valencia (VLC)	39.500 N -0.420 E	Multiwavelength-Lidar	J. L. Gómez-Amo

Table S6.2. Ground-based stations with estimated horizontal distance from HALO during the flights carried out during EMeRGe in Europe. For flight details see Sect. 3.3.

Flight number	Flight date	Ground-based station	Distance (km)
E-EU-03	11.07.	Bologna (BOL)	70
		Hohenpeissenberg (HOP)	20
		Ispra (IPR)	35
		Lecce (LCC)	350
		Naples (NAP)	170
		Rome (RME)	0
E-EU-04	13.07.	Hohenpeissenberg (HOP)	135
E-EU-05	17.07.	Cabauw (CBW)	185
		Cork (CRK)	390
		Lille (LLE)	40
		London (LND)	160
		Palaiseau (PLS)	115
E-EU-06	20.07.	Bologna (BOL)	45
		Ispra (IPR)	100
		Lecce (LCC)	395
		Naples (NAP)	170
		Rome (RME)	0
E-EU-07	24.07.	Barcelona (BRC)	55
		Hohenpeissenberg (HOP)	25
		Ispra (IPR)	155
		Madrid (MDR)	530
		Montsec (MSA)	185
		Montseny (MSY)	50
E-EU-08	26.07.	Cabauw (CBW)	90
		Hohenpeissenberg (HOP)	130
		Lille (LLE)	85
		London (LND)	80
		Palaiseau (PLS)	106
E-EU-09	28.07.	Barcelona (BRC)	50
		Granada (GRA)	435
		Hohenpeissenberg (HOP)	85
		Montsec (MSA)	50
		Montseny (MSY)	10
		Valencia (VLC)	60

S7 AOD measurements retrieved from AERONET sites for 500 nm and 675 nm

For 500 and 675 nm and in all EMeRGe target regions, the AOD retrieved from the AERONET sun-sky photometer stations in July 2017 is slightly lower than its 10-year-average, as for the results presented in Sect. 3.2. Except for the region of Eastern Spain, the relative differences between the AODs in July 2017 and their 10-year averages are larger than for the 1020 nm wavelength. The differences range from 15% to 31%. The AODs determined for BNL/Ruhr, Paris, Eastern Spain and Southern Great Britain are within the standard deviation of the 10-year-average AODs. In contrast, The AODs for the Po valley and Rome in 2017 are not within the standard deviation. The Po valley has poor data coverage at the wavelengths of 500 and 675 nm. The AOD retrieved at 675 nm in Rome are significantly lower than the 10-year-average.

The AERONET measurements at 500 and 675 nm indicate that the AODs over most EMeRGe target regions in July 2017 are representative. Further wavelengths are not suitable for a comparison due to the low data coverage in the 2009 to 2019 time period.

Table S7.1. AERONET stations used for the assessment of the aerosol load in six targeted regions of EMeRGe in Europe

EMeRGe target region	Station
Paris	Palaiseau Paris
BNL/Ruhr	Brussels Cabauw Lille Jülich
Southern Great Britain	Bayfordbury Chilbolton
Eastern Spain	Burjassot Montsec Palma de Mallorca
Rome	Rome Tor Vergata
Po Valley	Modena Sirmione

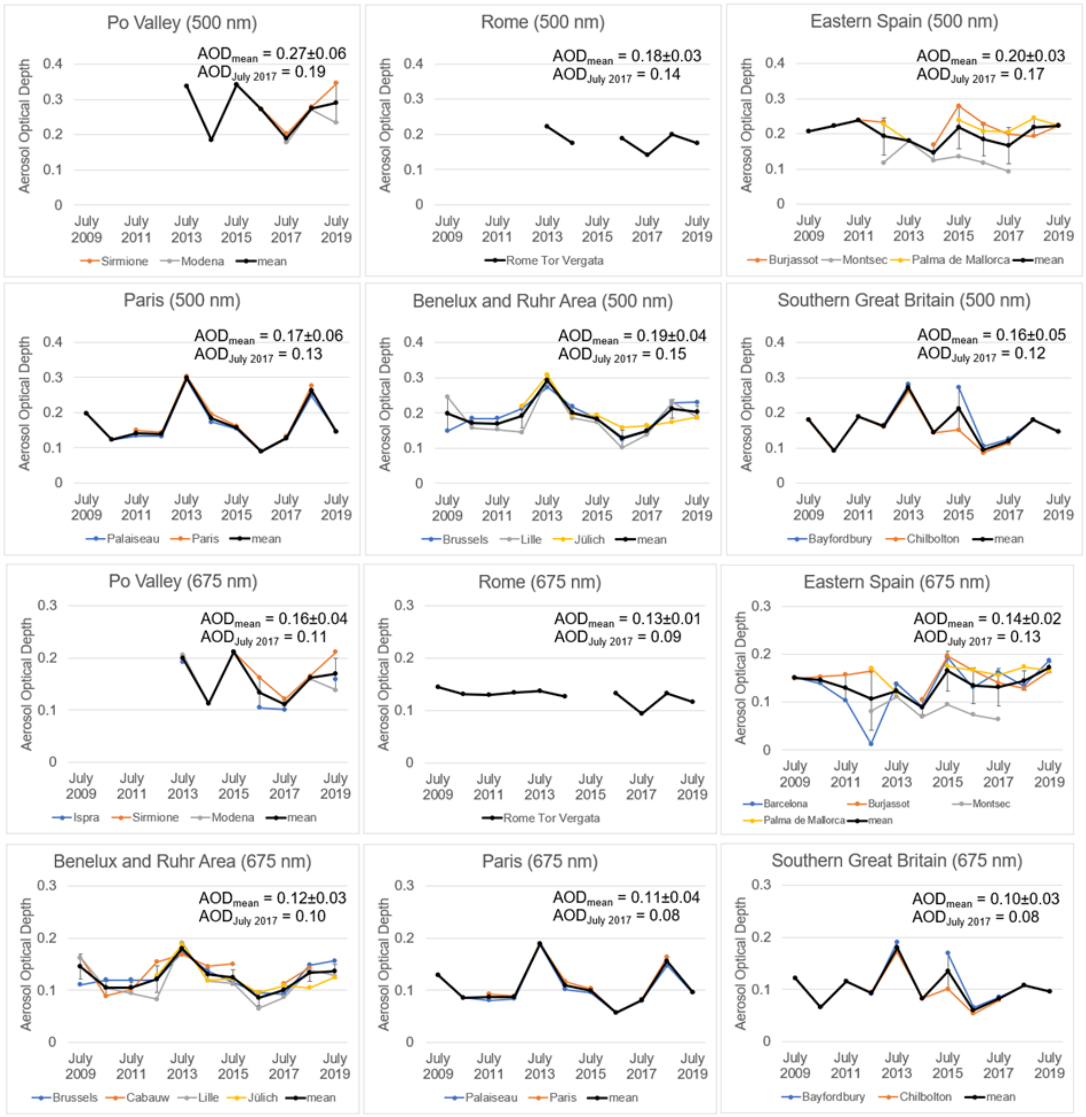

Figure S7.1. AODs derived at 500 and 675 nm for AERONET stations in all six target regions of EMeRGe in Europe. Black lines show mean AOD values. The AODs derived for July 2017 and the 2009 to 2019 average are shown on each diagram. The AODs from July 2017 are representative of the average AODs from 2009 to 2019.

S8 Coordinates of the MPC target areas shown in Figure 4

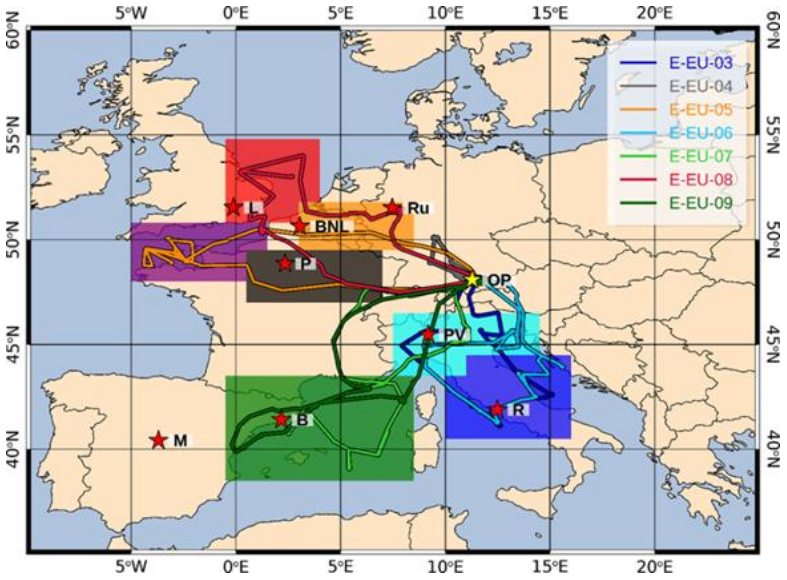

English Channel (purple)
Longitude: [-5.0, 0.5, 0.5, 1.5, 1.5, -5.0, -5.0]
Latitude: [48.0, 48.0, 49.5, 49.5, 50.8, 50.8, 48.0]
North Sea (red)
Longitude: [-0.5, 3.0, 3.0, 4.0, 4.0, -0.5, -0.5]
Latitude: [50.8, 50.8, 51.8, 51.8, 54.8, 54.8, 50.8]
Benelux/Ruhr (orange)
Longitude: [3.0, 49.5]
Latitude: [8.5, 51.8]
Paris (black)
Longitude: [0.5, 47.0]
Latitude: [7.0, 49.5]
Po Valley (cyan)
Longitude: [7.5, 11.0, 11.0, 14.5, 14.5, 7.5, 7.5]
Latitude: [43.5, 43.5, 44.5, 44.5, 46.5, 46.5, 43.5]
Central Italy (blue)
Longitude: [10.0, 16.0, 16.0, 11.0, 11.0, 10.0, 10.0]
Latitude: [40.5, 40.5, 44.5, 44.5, 43.5, 43.5, 40.5]
East Mediterranean (green)
Longitude: [0.5, 38.5]
Latitude: [8.5, 43.5]

S9 Details of selected flights tracks and flight routes

Table S9.1. Details of the EMeRGe flights in Flight route 1

Flight route 1	E-EU-03	E-EU-06
Alps	ca. 10:20 UTC FL170, 5100 m ca. 15:50 UTC FL 170-240, 5100-7300 m	ca 9:20 UTC FL 170-110, 5100-3300 m 16:20 UTC FL300, 9100 m
MPC Po Valley	10:30 UTC FL110, 3300m	shuttles 9:39 UTC and 10:00 UTC FL15/50/100: 450/1500/3000 m 11:50-12:10 UTC; FL:25, 750 m
Mediterranean coast of Italy	10:50 UTC FL90, 2700 m	12:20 UTC FL30, 900 m
Shuttle upwind Rome	12:00 UTC FL40/110/150 1200/3300/4000 m	13:00 UTC FL15/50/100 450/1500/3000 m
MPC Rome	13:30 UTC; FL 110,3300 m	14:00 UTC FL 100, 3000m
Adriatic coast	shuttle 13:42 UTC, FL150/110/40 4600/3300/900 m to the North FL30, 900 m	shuttle 14:15 UTC FL15/50/100 450/1500/3000 m Croatian coast shuttle 15:15 UTC FL15/50/100; 450/1500/3000 m
Munich		16:50-17:30 UTC Special landing ca 1000 m

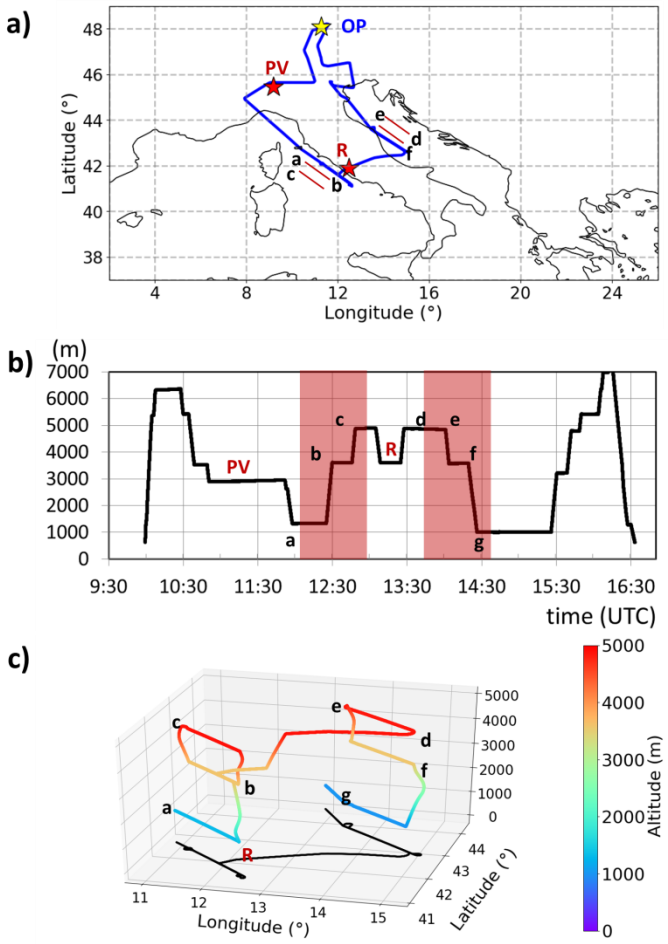

Figure S9.1. Details of the E-EU-03 track on the 11 July 2017. Two shuttles took place upwind Rome (R) and along the Adriatic coast and are marked with red lines on the map in a) as red shaded areas on the altitude diagram in b), as 3-D depiction in c). The flight track during the shuttles is shown in grey. The flight track in a) is coloured as in Fig. 4 and the EMeRGe MPC targets in red. Main changes in course and altitude are marked (a-g) on the graphs for reference. OP indicates the position of the HALO base.

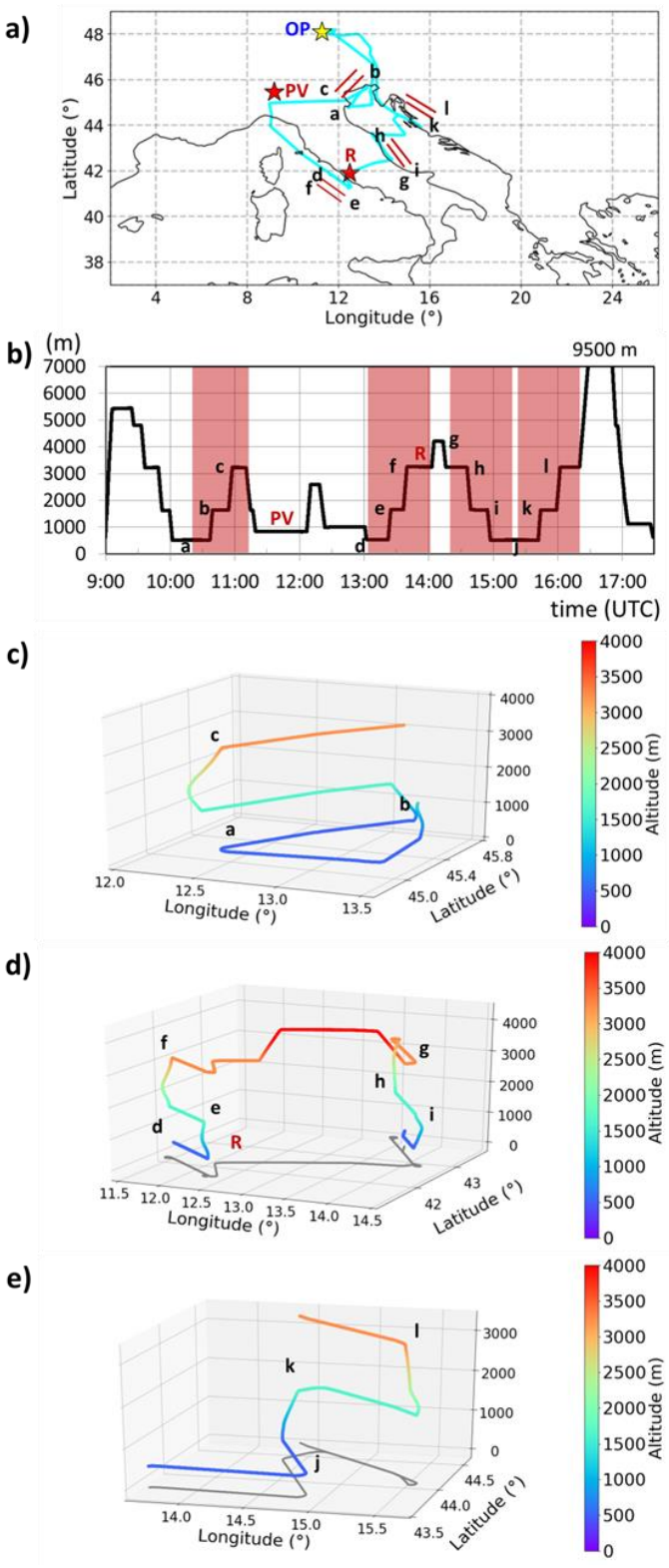

Figure S9.2. Details of the E-EU-06 track on the 20 July 2017. Three shuttles took place downwind of the Po Valley (PV), upwind Rome (R) and along the Adriatic coast are marked with red lines on the map in a) as red shaded areas on the altitude diagram in b), and as a 3-D depiction in c), d) and e). The flight tracks during the shuttles d) and e) are shown in grey. The flight track in a) is coloured as in Fig. 4 and the EMeRGe MPC targets in red. Main changes in course and altitude are marked (a-l) on the graphs for reference. OP indicates the position of the HALO base.

187 **Table S9.2.** Details of the EMeRGe flights in Flight route 2 and special case E-EU-04

Flight route 2	**E-EU-05**	**E-EU-08**
MPC BNL/Ruhr	ca. 10:40 UTC FL180, 5500 m	ca. 12:45 -14:30 UTC ~FL80 cloudy Shuttle 13:20 UTC FL 30/50/80 900/1500/2400 m
MPC London	English Channel 12:00-16:45 UTC FL15-80, 400-2400 m	Two shuttles (North Sea) 10:14 UTC; FL20/40/200: 600/1200/600 m 13:05 UTC; FL30/50/80, 900/1500/2400 m
MPC Paris	17:00 UTC FL70, 2100 m	8:40 UTC FL70, 2100 m
Munich		ca 15:00 UTC Special landing ca 1000 m

188

E-EU-04	
FAAM_HALO intercomparison exercise	ca. 10:55 UTC entering race track FL90 (ca 2700 m) FL150/FL90/FL40 4500/2700/1200 m ca 12:51 UTC end exercise
Intercontinental transport pollution/Canada fires	ca. 13:20-14:00 UTC FL230, 7100 m
Munich	ca 14:40 UTC, ca FL30, 1000 m

189

190

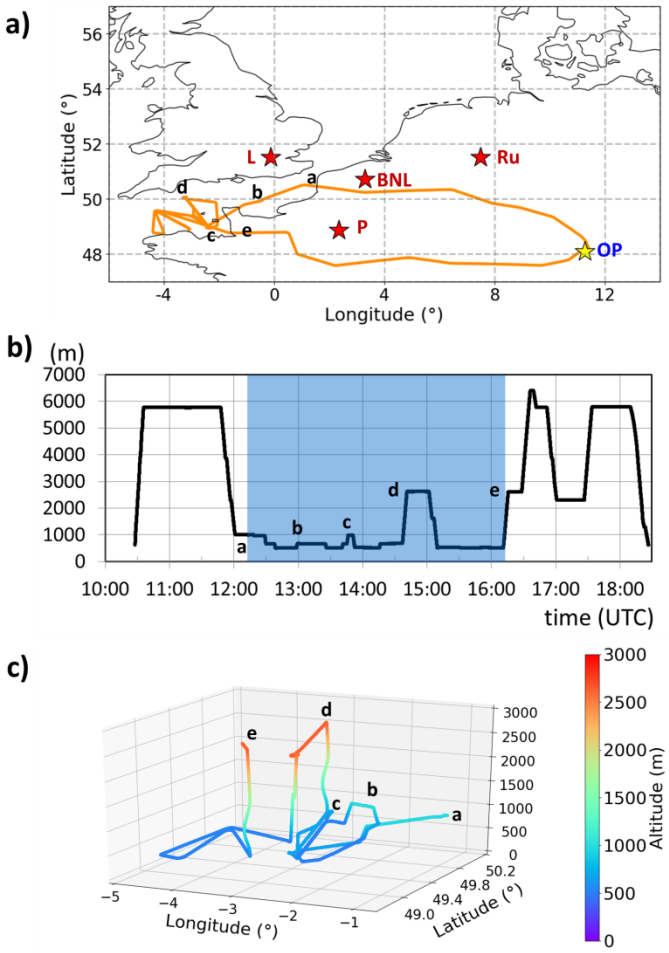

Figure S9.3. Details of the E-EU-05 track on the 17 July 2017. The probing area of the outflow of London over the English Channel is shown in a), as a blue shaded area on the altitude diagram in b), and as a 3-D depiction in c). The flight track in a) is coloured as in Fig. 4 and the EMeRGe MPC targets marked in red. Main changes in course and altitude are marked (a-e) on the graphs for reference. OP indicates the position of the HALO base.

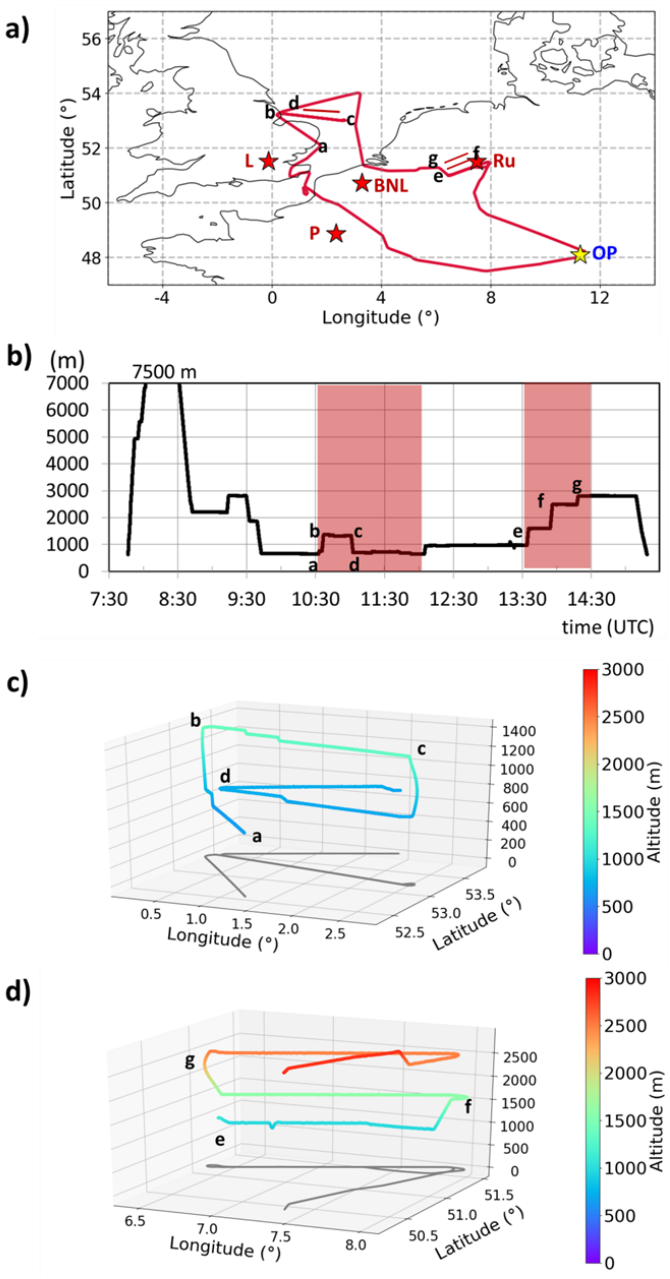

197

198 **Figure S9.4.** Details of the E-EU-08 flight on the 26 July 2017. The position of the shuttles downwind London and the BNL/
199 Ruhr area are indicated in red on the map in a), marked by the red shaded areas in b), and as a 3-D depiction in c) and d). The
200 flight tracks during the shuttles are shown in c) and d) in grey. On the map in a) the EMeRGe MPC targets are marked in red
201 and the flight track coloured as in Fig.4. Main changes in course and altitude are marked (a-g) on the graphs for reference. OP
202 indicates the position of the HALO base.

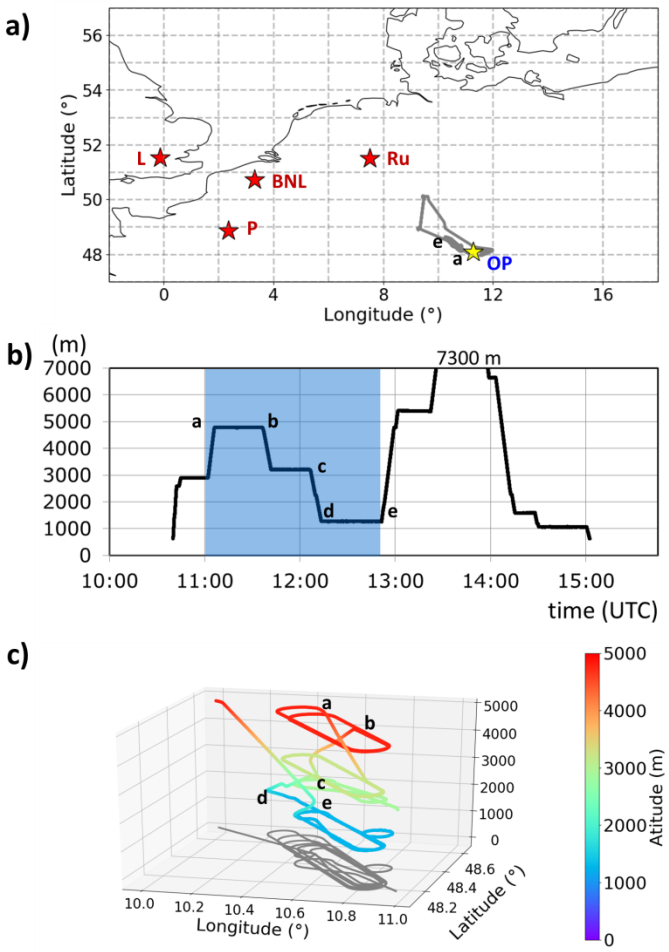

Figure S9.5. Details of the E-EU-04 flight on the 13 July 2017. The flight track coloured as in Fig. 4 is shown on the map in a). The HALO-FAAM intercomparison exercise is indicated by the blue shaded area in b), and as a 3-D depiction in c). The flight track is shown in c) in grey. In a), the position of the nearest MPC targets is indicated in red. Main changes in course and altitude are marked (a-d) on the graphs for reference. OP indicates the position of the HALO base.

208 **Table S9.3.** Details of the EMeRGe flights in Flight route 3.

Flight route 3	**E-EU-07**	**E-EU-09**
Po Valley	ca. 10:20 UTC FL60, 1800m	10-11 UTC FL 240,7300m
Outflow South France (Marseille fires)	shuttle11:35 UTC FL90/50/15, 2700/1500/450m	shuttle 10:55 UTC FL100/30/15, 300/100/450m 16:00 UTC FL90, 2700m
MPC Barcelona	shuttle 12:40 UTC FL50/15 1500m/450m	shuttle 15 UTC coast of Barcelona FL15/50/90 3000/900/450m
Mediterranean	ca. 13:30 UTC FL15-50, 450-1500m shuttle 14:50 UTC NW of Sardinia FL15/50/110 450/1500/3300m	11:50 UTC FL60, 1800m shuttle 13:45 UTC East of Valencia FL100/30/15 3000/900/450m,
Central France	16:40 UTC FL 200, 6100m	16:40 UTC FL 200, 6100m
Munich	----	18:00-18:30 UTC Special landing ca 1000m

209

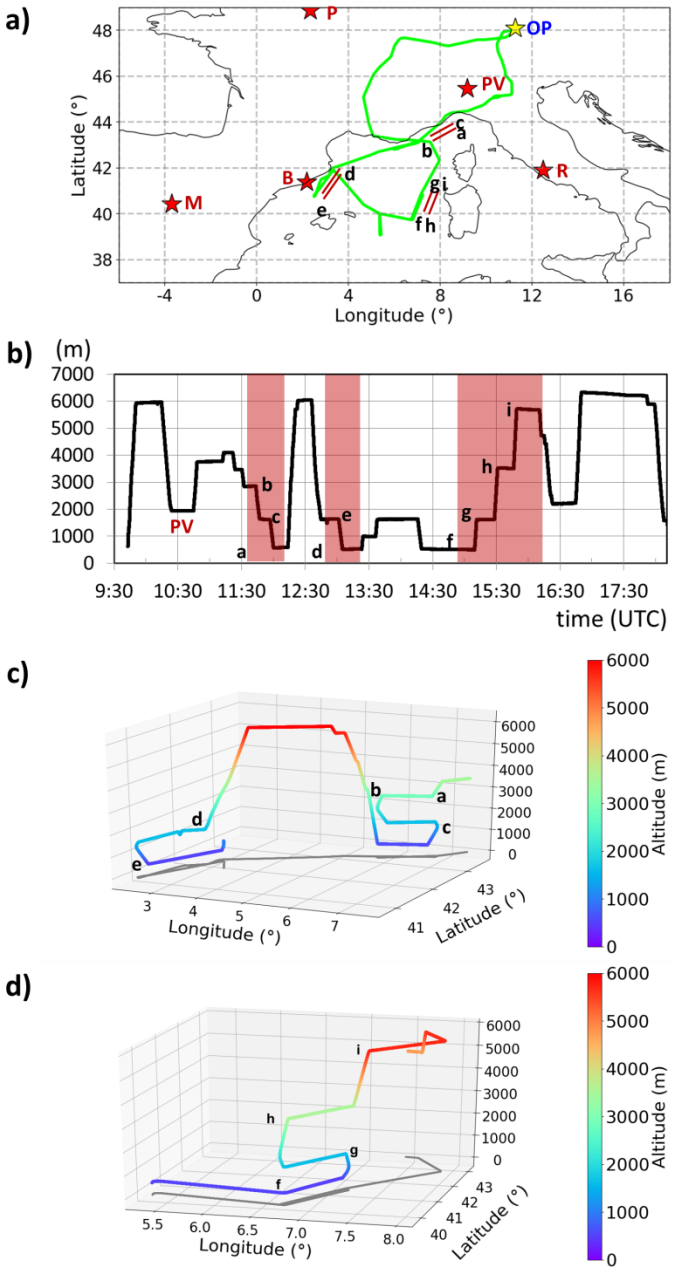

Figure S9.6. Details of the E-EU-07 flight on the 24 July 2017. The position of the shuttles taking place downwind of Marseille, Barcelona and the West coast of Sardinia are indicated in red on the map in a), marked by the red shaded areas in b), and as 3-D depicted in c) and d). The flight tracks during the shuttles are shown in c) and d) in grey. In a) the EMeRGe MPC targets are marked in red and the flight track coloured as in Fig. 4. Main changes in course and altitude are marked (a-i) on the graphs for reference. OP indicates the position of the HALO base.

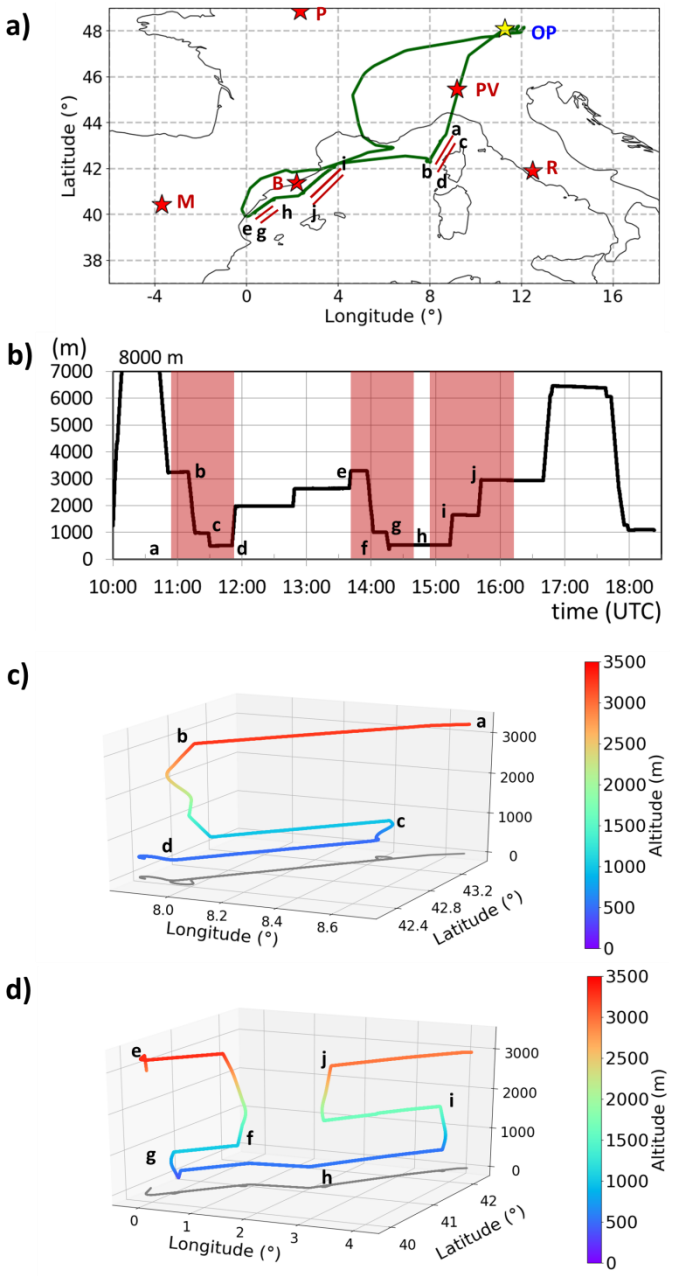

Figure S9.7. Details of the E-EU-09 flight on the 28 July 2017. The position of the shuttles taking place downwind of Marseille, Barcelona and the East coast of Spain are indicated in red on the map in a), marked by the red shaded areas in b), and 3-D depicted in c) and d). The flight tracks during the shuttles are shown in c) and d) in grey. In a) the EMeRGe MPC targets are marked in red and the flight track coloured as in Fig. 4. Main changes in course and altitude are marked (a-j) on the graphs for reference. OP indicates the position of the HALO base.

S10 Selected measured average concentrations for all the EMeRGe flights

Table S10.1. Mean concentrations (mean), median (med) and quartiles (25^{th} 75^{th}) of selected measured trace gases and aerosol particles for the EMeRGe flights not presented in the manuscript. n.a. non-available ^{x}HCHO: HCHO from PTRMS measurements; *HCHO: HCHO from miniDOAS measurements; N_{CN}: $\mathbf{N_{D>250nm}}$ particle with D> 10 nm, and D>250 nm, respectively (inlet cut-off 1.5 to 3 µm depending on height); BCm: black carbon mass concentration; BCn: black carbon number concentration; OA: Organic aerosol. Note that NCN, N_D, BCm, BCn, OA, NO_3^-, SO_4^{2-}, NH_4^+ and Cl^- are given for standard temperature and pressure conditions.

E-EU-03	<2000 m				2000-4000 m				>4000 m				
species	mean	med	25^{th}	75^{th}	mean	med	25^{th}	75^{th}	mean	med	25^{th}	75^{th}	Unit
O_3	61.9	63.4	57.4	68.6	60.1	60.1	56.8	63.3	73.7	75.5	63.8	83.9	ppbV
CO	96.7	99.9	86.7	104.5	80.8	85.1	75.9	89	89	88.7	83	95.6	ppbV
NO	144	135	108	167	66	57	39	82	38	36	28	44	pptV
NO_y	1561	1414	880	2035	576	599	340	751	410	409	355	470	pptV
HONO	51	49	35	65	42	25	12	40	5	5	4	6	pptV
NO_2	363	331	120	475	86	60	51	73	44	34	29	49	pptV
*HCHO	1983	2006	1322	2503	751	737	547	914	342	338	288	382	pptV
RO_2^*	58	64	37	78	46	43	34	62	30	26	11	43	pptV
SO_2	n.a.	n.a.	n.a.	n.a.	n.a.	n.a.	n.a.	n.a.	n.a.	n.a.	n.a.	n.a.	pptV
N_{CN}	4478	4309	2232	5951	2142	1835	1084	2777	974	877	771	1031	cm^{-3}
$N_{D>250nm}$	103.3	106.1	55	126.8	48.4	36.6	13.2	82.3	9.8	9	6	11.8	cm^{-3}
BCm	0.215	0.196	0.118	0.279	0.048	0.03	0.01	0.065	0.01	0.005	0.002	0.01	$\mu g\ m^{-3}$
BCn	97	96	54	128	23	16	6	36	4	3	2	5	cm^{-3}
OA	1.992	2.157	1.236	2.543	1.424	1.264	0.549	2.213	0.394	0.394	0.307	0.478	$\mu g\ m^{-3}$
NO_3^-	0.224	0.114	0.07	0.21	0.187	0.184	0.067	0.272	0.044	0.038	0.028	0.05	$\mu g\ m^{-3}$
SO_4^{2-}	1.088	1.115	0.783	1.469	0.386	0.263	0.161	0.551	0.113	0.108	0.092	0.127	$\mu g\ m^{-3}$
NH_4^+	0.521	0.497	0.329	0.659	0.289	0.288	0.139	0.399	0.08	0.072	0.058	0.085	$\mu g\ m^{-3}$
Cl^-	0.03	0.029	0.018	0.039	0.021	0.02	0.017	0.025	0.01	0.01	0.01	0.01	$\mu g\ m^{-3}$
C_3H_6O	2375	2473	1901	2906	1560	1613	1210	1933	1656	1691	1512	1863	pptV
CH_3CN	123	121	104	138	118	120	104	129	140	139	125	156	pptV
C_5H_8	100	93	68	116	66	64	53	75	77	68	57	90	pptV
C_6H_6	115	123	55	162	40	31	24	46	28	27	24	31	pptV
C_7H_8	45	44	23	60	23	21	18	25	28	25	20	31	pptV
^{x}HCHO	2190	2197	1364	2841	816	770	562	1018	469	460	385	551	pptV
$C_2H_2O_2$	183	158	125	219	120	89	58	139	93	90	71	122	pptV
$C_3H_4O_2$	1235	1231	1106	1346	988	806	621	1126	790	758	623	1013	pptV

230

E-EU-04	<2000 m				2000-4000 m				>4000 m				
species	mean	med	25^{th}	75^{th}	mean	med	25^{th}	75^{th}	mean	med	25^{th}	75^{th}	Unit
O_3	45	45	42	48	55	54	51	60	67	69	59	74	ppbV
CO	86	86	84	89	79	79	78	80	94	89	87	99	ppbV
NO	310	274	220	375	50	40	30	50	41	34	27	43	pptV
NO_y	2078	1885	1651	2419	345	234	166	427	294	273	233	327	pptV
HONO	75	73	68	82	19	17	11	24	11	11	8	13	pptV
NO_2	722	544	423	964	72	59	49	78	32	32	28	35	pptV
*HCHO	1251	1196	1147	1431	375	347	314	411	169	168	150	182	pptV
RO_2^*	21	24	8	30	29	29	20	36	19	18	8	28	pptV
SO_2	181	176	154	202	111	107	100	119	107	106	97	115	pptV
N_{CN}	9619	7905	4444	13898	928	691	587	849	1701	1172	980	1632	cm^{-3}
$N_{D>250nm}$	68.8	67.6	54.4	80.7	7.6	6	4.7	8.1	8.9	7.3	5.8	10	cm^{-3}
BCm	0.08	0.06	0.04	0.09	0.01	0.00	0.00	0.01	0.01	0.00	0.00	0.01	$\mu g\ m^{-3}$
BCn	44	39	31	52	3	2	1	4	3	2	1	4	cm^{-3}
OA	1.47	1.45	1.33	1.59	0.37	0.33	0.27	0.40	0.56	0.51	0.41	0.71	$\mu g\ m^{-3}$
NO_3^-	0.73	0.70	0.54	0.82	0.13	0.03	0.03	0.04	0.04	0.04	0.03	0.05	$\mu g\ m^{-3}$
SO_4^{2-}	0.63	0.62	0.55	0.71	0.18	0.18	0.14	0.22	0.10	0.09	0.07	0.12	$\mu g\ m^{-3}$
NH_4^+	0.49	0.48	0.40	0.55	0.15	0.08	0.05	0.15	0.08	0.07	0.07	0.10	$\mu g\ m^{-3}$
Cl^-	0.05	0.04	0.03	0.06	0.04	0.03	0.03	0.05	n.a.	n.a.	n.a.	n.a.	$\mu g\ m^{-3}$
C_3H_6O	1356	1351	1261	1442	1376	1388	1314	1435	1682	1614	1543	1716	pptV
CH_3CN	69	70	61	80	98	100	88	112	134	132	108	149	pptV
C_5H_8	83	77	63	96	70	68	55	84	75	72	61	90	pptV
C_6H_6	41	38	32	48	30	30	26	35	31	28	23	35	pptV
C_7H_8	40	38	29	48	26	22	19	28	22	21	18	27	pptV
^{x}HCHO	1215	1175	1017	1378	518	515	448	594	487	469	385	607	pptV
$C_2H_2O_2$	168	150	112	208	98	65	28	103	68	71	19	112	pptV
$C_3H_4O_2$	1108	1150	844	1303	806	641	409	866	560	453	250	829	pptV

231

E-EU-05	<2000 m				2000-4000 m				>4000 m				
species	mean	med	25th	75th	mean	med	25th	75th	mean	med	25th	75th	Unit
O_3	32	33	30	35	44	43	36	50	61	58	52	71	ppbV
CO	79	80	76	83	65	63	54	73	63	63	57	67	ppbV
NO	173	109	91	150	57	39	24	58	34	33	27	40	pptV
NO_y	2725	2455	2056	3025	1115	931	751	1175	577	547	280	822	pptV
HONO	8	3	0	15	4	3	0	7	0	0	0	0	pptV
NO_2	275	258	186	339	87	49	34	149	27	29	25	30	pptV
*HCHO	1004	1010	926	1107	613	425	370	914	209	204	185	231	pptV
RO_2^*	25	24	16	31	27	26	19	32	28	28	15	40	pptV
SO_2	111	84	61	116	52	49	39	62	44	42	34	52	pptV
N_{CN}	3545	2833	1843	4555	1681	578	402	2855	852	692	592	935	cm^{-3}
$N_{D>250nm}$	89.9	84.4	45.8	127.8	25.3	9.3	5.1	50.3	3.4	2.6	1.8	3.8	cm^{-3}
BCm	0.11	0.09	0.05	0.14	0.04	0.01	0.00	0.07	0.00	0.00	0.00	0.00	$\mu g\ m^{-3}$
BCn	52	50	28	69	22	4	2	47	2	2	1	3	cm^{-3}
OA	1.44	1.49	0.98	1.86	2.20	2.28	0.39	3.79	0.24	0.21	0.16	0.27	$\mu g\ m^{-3}$
NO_3^-	0.73	0.49	0.24	1.11	0.65	0.49	0.39	0.70	0.02	0.02	0.02	0.03	$\mu g\ m^{-3}$
SO_4^{2-}	0.71	0.69	0.42	0.88	0.29	0.19	0.16	0.51	0.19	0.18	0.12	0.25	$\mu g\ m^{-3}$
NH_4^+	0.54	0.49	0.30	0.73	0.32	0.32	0.09	0.42	0.08	0.08	0.06	0.09	$\mu g\ m^{-3}$
Cl^-	0.04	0.04	0.02	0.06	0.03	0.03	0.02	0.04	n.a.	n.a.	n.a.	n.a.	$\mu g\ m^{-3}$
C_3H_6O	n.a.	n.a.	n.a.	n.a.	n.a.	n.a.	n.a.	n.a.	n.a.	n.a.	n.a.	n.a.	pptV
CH_3CN	n.a.	n.a.	n.a.	n.a.	n.a.	n.a.	n.a.	n.a.	n.a.	n.a.	n.a.	n.a.	pptV
C_5H_8	n.a.	n.a.	n.a.	n.a.	n.a.	n.a.	n.a.	n.a.	n.a.	n.a.	n.a.	n.a.	pptV
C_6H_6	n.a.	n.a.	n.a.	n.a.	n.a.	n.a.	n.a.	n.a.	n.a.	n.a.	n.a.	n.a.	pptV
C_7H_8	n.a.	n.a.	n.a.	n.a.	n.a.	n.a.	n.a.	n.a.	n.a.	n.a.	n.a.	n.a.	pptV
^{x}HCHO	n.a.	n.a.	n.a.	n.a.	n.a.	n.a.	n.a.	n.a.	n.a.	n.a.	n.a.	n.a.	pptV
$C_2H_2O_2$	161	144	106	201	82	59	15	96	66	69	19	109	pptV
$C_3H_4O_2$	1128	1175	884	1318	753	626	416	848	613	585	260	822	pptV

232

E-EU-07	<2000 m				2000-4000 m				>4000 m				
species	mean	med	25th	75th	mean	med	25th	75th	mean	med	25th	75th	Unit
O_3	47	46	41	54	51	51	44	56	64	62	58	69	ppbV
CO	105	101	92	109	115	102	92	110	103	106	97	110	ppbV
NO	189	136	110	265	120	67	47	121	283	49	37	72	pptV
NO_y	1335	919	743	1823	904	564	390	729	1140	451	393	604	pptV
HONO	25	16	7	34	9	5	0	16	5	0	0	5	pptV
NO_2	202	172	144	236	161	61	27	152	52	53	24	67	pptV
*HCHO	973	832	720	1245	438	382	323	450	280	265	140	380	pptV
RO_2^*	39	40	29	49	35	33	19	48	26	19	5	32	pptV
SO_2	224	177	118	262	78	66	48	91	60	57	44	73	pptV
N_{CN}	6508	3446	2367	6854	2919	1995	1235	2907	4350	3123	1518	5453	cm^{-3}
$N_{D>250nm}$	99.2	65.1	33.4	111.1	94	15.7	7.8	65.1	11.4	6.1	3.9	11.1	cm^{-3}
BCm	0.12	0.07	0.04	0.12	0.10	0.02	0.01	0.04	0.01	0.01	0.00	0.01	$\mu g\ m^{-3}$
BCn	55	37	21	62	46	9	3	20	5	4	2	6	cm^{-3}
OA	2.34	1.68	1.21	3.12	1.30	0.59	0.36	2.03	0.44	0.35	0.26	0.45	$\mu g\ m^{-3}$
NO_3^-	0.31	0.15	0.08	0.49	0.18	0.08	0.03	0.26	0.07	0.04	0.03	0.06	$\mu g\ m^{-3}$
SO_4^{2-}	0.82	0.85	0.38	1.16	0.25	0.13	0.07	0.30	0.10	0.08	0.05	0.13	$\mu g\ m^{-3}$
NH_4^+	0.46	0.43	0.29	0.62	0.31	0.23	0.15	0.51	0.09	0.08	0.06	0.09	$\mu g\ m^{-3}$
Cl^-	0.09	0.05	0.02	0.16	0.04	0.04	0.02	0.05	0.10	0.10	0.10	0.10	$\mu g\ m^{-3}$
C_3H_6O	1734	1678	1400	1974	1580	1399	1244	1644	1535	1605	1364	1691	pptV
CH_3CN	124	117	103	131	191	139	119	154	132	134	117	149	pptV
C_5H_8	92	69	57	114	170	80	58	108	66	62	54	70	pptV
C_6H_6	81	66	43	94	71	39	29	54	31	29	24	35	pptV
C_7H_8	51	44	34	61	69	26	20	38	32	31	18	43	pptV
^{x}HCHO	1391	1211	903	1684	1015	682	468	925	467	446	385	527	pptV
$C_2H_2O_2$	221	201	141	268	192	116	54	259	132	88	22	172	pptV
$C_3H_4O_2$	1603	1380	1140	1999	1430	808	591	1841	1012	616	430	1255	pptV

233

E-EU-09	<2000 m				2000-4000 m				>4000 m				
species	mean	med	25th	75th	mean	med	25th	75th	mean	med	25th	75th	Unit
O_3	46	45	41	53	59	60	51	69	54	53	46	62	ppbV
CO	94	94	89	103	104	102	84	129	65	62	60	64	ppbV
NO	148	135	101	190	84	80	67	95	39	35	27	46	pptV
NO_y	1151	1051	851	1287	827	907	357	1169	331	281	189	379	pptV
HONO	n.a.	n.a.	n.a.	n.a.	n.a.	n.a.	n.a.	n.a.	n.a.	n.a.	n.a.	n.a.	pptV
NO_2	n.a.	n.a.	n.a.	n.a.	n.a.	n.a.	n.a.	n.a.	n.a.	n.a.	n.a.	n.a.	pptV
*HCHO	n.a.	n.a.	n.a.	n.a.	n.a.	n.a.	n.a.	n.a.	n.a.	n.a.	n.a.	n.a.	pptV
RO_2^*	46	48	35	62	53	55	39	66	13	10	1	20	pptV
SO_2	301	287	193	384	203	204	98	281	73	68	54	85	pptV
N_{CN}	4080	3921	2960	4813	2634	3025	865	3493	2282	1465	1125	3191	cm^{-3}
$N_{D>250nm}$	66	65.1	42.8	78.8	133.9	129	12.6	251.2	1.2	0.6	0.2	1.5	cm^{-3}
BCm	0.12	0.10	0.07	0.15	0.33	0.32	0.02	0.57	0.00	0.00	0.00	0.00	$\mu g\ m^{-3}$
BCn	57	52	40	69	97	102	7	165	1	0	0	1	cm^{-3}
OA	2.41	1.89	1.06	3.58	5.47	6.11	4.61	7.27	0.25	0.23	0.19	0.31	$\mu g\ m^{-3}$
NO_3^-	0.22	0.17	0.13	0.27	0.34	0.32	0.23	0.44	n.a.	n.a.	n.a.	n.a.	$\mu g\ m^{-3}$
SO_4^{2-}	0.97	0.66	0.46	1.45	0.36	0.34	0.20	0.50	0.16	0.17	0.12	0.21	$\mu g\ m^{-3}$
NH_4^+	0.45	0.41	0.28	0.60	0.36	0.34	0.26	0.45	0.12	0.12	0.10	0.13	$\mu g\ m^{-3}$
Cl^-	0.05	0.05	0.04	0.06	0.05	0.05	0.04	0.06	0.04	0.04	0.03	0.04	$\mu g\ m^{-3}$
C_3H_6O	1774	1610	1419	2022	1811	1851	1319	2302	915	814	774	955	pptV
CH_3CN	126	126	111	140	168	169	147	192	133	131	118	141	pptV
C_5H_8	72	69	55	84	68	63	54	75	64	60	55	67	pptV
C_6H_6	79	72	54	96	80	81	54	104	33	31	25	35	pptV
C_7H_8	35	28	20	38	25	22	19	27	23	18	17	28	pptV
^xHCHO	1418	1369	1209	1555	1136	1201	788	1406	433	421	341	493	pptV
$C_2H_2O_2$	n.a.	n.a.	n.a.	n.a.	n.a.	n.a.	n.a.	n.a.	n.a.	n.a.	n.a.	n.a.	pptV
$C_3H_4O_2$	n.a.	n.a.	n.a.	n.a.	n.a.	n.a.	n.a.	n.a.	n.a.	n.a.	n.a.	n.a.	pptV

S11 Backward trajectories

Air mass back trajectories for the EMeRGe flights are calculated with the FLEXTRA 5.0 trajectory model developed by Stohl et al., (1999) and using the European Centre for Medium-Range Forecasts (ECMWF) operational data set ERA5 meteorological data at 0.25° horizontal resolution. Trajectories are started every 1 minute of flight time and reach back 10 days. The general content of the model output has been enhanced by adding manually other parameters after the simulations (troph, tropp, blh, sp, surf, cwc) which provide additional information over the BL conditions along the trajectory.

There are two sets of data:

1. Original trajectories of the FLEXTRA runs at the ~10 min temporal resolution along the flight tracks.

2. Interpolated trajectories at a strict 5 min temporal resolution, linearly interpolated from the original trajectories. In the interpolated trajectories the timestamps are the same for all releases / trajectories and the temporal resolution is higher.

S12 General description of MECO(n)

The MECO(n) model system (Kerkweg and Jöckel, 2012a,b, Hofmann et al., 2012, Mertens et al.,2016, Kerkweg et al., 2018) consists of the global chemistry-climate model EMAC and the regional chemistry-climate model COSMO-CLM/MESSy. The nesting of COSMO in EMAC is performed during runtime. The boundary conditions which are necessary for the regional model instances are provided by the next coarser resolved model instance. New boundary conditions are provided at every time step of the driving model, and specific events of long-range transport (e.g. from biomass burning) are captured well in the regional refinements.

S12.1 Model dynamics

EMAC and COSMO-CLM/MESSy are chemistry-climate models which calculate the atmospheric dynamics by solving the primitive equations. The global model EMAC applies the spectral core of the global circulation model ECHAM5. The Newtonian relaxation (nudging) is performed in spectral space for the prognostic variables divergence, vorticity, temperature, and the (logarithm of the) surface pressure. This applied for 48, 6, 24, and 24 h, respectively for the EMeRGe simulations (see Jöckel et al., 2016). The nudging data are linearly interpolated during updates every 6 hours. Usually, ERA-Interim, ECMWF operational analysis or ERA-5 data are used for the nudging (see below). The regional refinements are not nudged towards ECMWF or any other data. As in classical downscaling applications the prognostic variables are relaxed towards the global model (or coarser resolved regional refinements) at the lateral and top boundaries. This means that the regional model can develop to a certain degree its own dynamics.

S.12.2 Chemical kinetics

In total, the mechanism is described by 298 reactions of 188 species. The chemical species and reactions are as described by Jöckel et al. (2016). Basic gas-phase chemistry of ozone, methane, and odd nitrogen, alkanes and alkenes up to C4 are included. Alkynes and aromatics are not considered. Halogen chemistry includes bromine and chlorine species. For the chemistry of isoprene and selected non-methane hydrocarbons (NMHCs), version 1 of the Mainz Isoprene Mechanism (MIM1) based on Pöschl et al. (2000) is used. Heterogeneous reactions of dinitrogen pentoxide (N_2O_5), halogen nitrates ($ClNO_3$, $BrNO_3$), and hypohalous acids (HOCl, HOBr) are also included. All Hg reactions are switched off.

NO_y is defined as: $NO_y = BrNO_2 + BrNO_3 + ClNO_2 + CLNO_3 + HNO + HONO + HNO_3 + HNO_4 + IC_3H_7NO_3 + ISON + LC_4H_9NO_3 + N + 2 \cdot N_2O_5 + NO + NO_2 + NO_3 + {NO_3}^-_{cs} + PAN$.

${NO_3}^-_{cs}$ is a residual aerosol as reaction product of the heterogeneous reaction of N_2O_5: $N_2O_5 \rightarrow 2\ {NO_3}^-_{cs} + 2{H^+}_{cs}$

RO_2 is defined as: $RO_2 = HO_2 + CH_3O_2 + ISOOH + CH_3CO_3 + CH_3COCH_2O_2 + C_2H_5O_2$

S12.3 Aqueous phase chemistry, scavenging, wet and dry deposition

As in Jöckel et al. (2016) aqueous-phase chemistry in clouds and wet deposition are simulated with the help of the combined explicit scavenging submodel SCAV (Tost et al., 2006a, 2007a, 2010), which calculates the uptake/release to/from the gas and aqueous phase and subsequent wet deposition. In contrast to more simplified schemes, dissociation and aqueous-phase redox reactions are also explicitly calculated, e.g. the sulphur (IV) to sulphur (VI) oxidation, such that the effective exchange between gas and liquid phase is taken into account. The scheme also includes nitric acid (HNO_3) uptake on. Wet deposition is calculated from the in-cloud (and subsequent conversion of in-cloud to in-precipitation) and in-precipitation chemical concentrations for both large-scale and convective clouds.

Dry deposition of chemical species is calculated using the big leaf approach as proposed by Wesely (1989). The implementation of this process in EMAC/MECO(n) is described in detail by Kerkweg et al. (2006).

290 **S12.4 Simulation set-up**

291 The simulations are performed using MECO(n) in a MECO(3) configuration, meaning three refinements of
292 COSMO-CLM/MESSy are embedded in EMAC: a) 50 km horizontal resolution, 131 x 121 horizontal grid
293 boxes, time step length = 240 s (CM50), b) 12 km horizontal resolution, 245 x 221 horizontal grid boxes, time
294 step length = 120 s (CM12) and c) 7 km resolution, 330 x 310 horizontal grid boxes, time step length = 60 s (CM7)
295

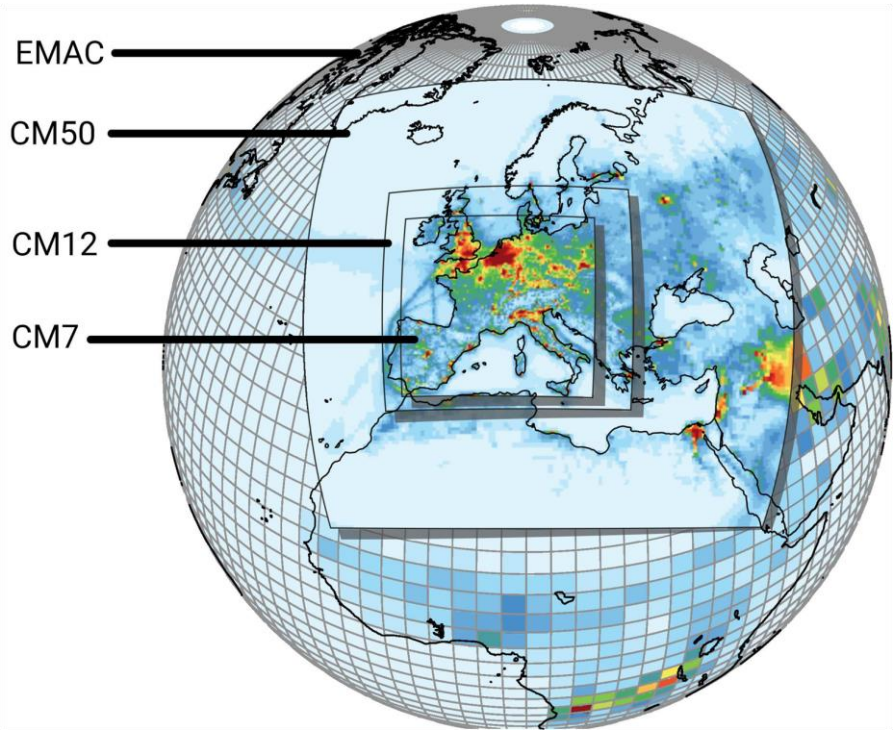

296 **Figure S12.1.** Definition of the computational domains of the MECO(3) set-up.

297 EMAC is applied at a horizontal spectral resolution of T42 (approx. 2.8° x 2.8°) and 90 vertical, terrain following
298 levels from the surface up to approx. 80 km. The time step length is 12 minutes. All COSMO-CLM/MESSy
299 refinements are applied with 40 terrain following vertical levels from the surface up to around 20 km. The results
300 of CM12 and CM7 were not significantly different.
301 The emission set-up of the reference simulation is the following:
302 • Long lived greenhouse gases (CO_2, N_2O, CH_4) and CFCs concentrations are relaxed to- wards prescribed
303 concentrations at surface following the RCP 8.5 emission inventory. These concentrations are zonally
304 averaged.
305 • Anthropogenic emissions according to the 4.3.1 emission inventory (monthly resolution for the year 2010).
306 • Emissions from biomass burning and agricultural waste burning following the RCP 8.5 emission inventory
307 (does not correspond the 'real biomass burning emissions in 2017).
308 • Emissions of NOx from soils and biogenic VOC are calculated depending on the meteorological conditions
309 following the parametrisations of Yienger and Levy (1995) and Guentheret al. (1995).
310 • Lightning NOx is parametrised according to Price and Rind (1994).
311

S12.5 Sensitivity experiments

- emerge3 b (CM50, CM12): Reference simulation with emissions as described above. Nudging of EMAC towards ERA-Interim.
- emerge3 s1 (CM50,CM12,CM7): CH_4 emissions from the EDGAR 4.2 FT emission inventory.
- emerge3 s3 (CM50,CM12): VEU2 emission inventory for anthropogenic emissions are applied for Europe instead of EDGAR 4.3.1
- emerge3 s4 (CM50,CM12): Dynamics in EMAC is nudged towards ECMWF operational analysis data instead of ERA-Interim
- emerge3 s5 (CM50,CM12): 50 instead of 40 vertical model layers increasing vertical resolution in the free troposphere
- emerge3 s6 (CM50, CM12): EDGAR 5.0 emissions for CO_2 and CH_4, diagnostic SO_2 tracer with reaction SO_2 + OH as only loss, additional budget terms for the kinetic calculations.

S12.6 Tagging method for source apportionment

The tagging method used for source apportionment is reported by Grewe et al., 2017 and Rieger et al., 2018. This method is an accounting system which follows the reaction pathways of emissions from different emission sectors. The source apportionment is made for O_3, CO, PAN, NO_y (without PAN), NMHC, OH and HO_2. In this study 12 categories are used (Table S12.1).

Table S12.1. Definition of the tagging categories used for EMeRGe.

Tagging Category	Description
Stratosphere	downward Transport from the stratosphere
CH_4	degradation of CH_4
Biogenic	biogenic emissions (soil-NOx, biogenic VOCs and CO)
N_2O	degradation of N_2O
Biomass Burning	biomass burning emissions
Lightning	lightning emissions (NOx)
Shipping	shipping emissions (IPCC codes 1A3d+1C2)
Aviation	aviation emissions
Anth. non-traffic EU	emissions of IPCCs sectors 1A1a, 1A1b+1B2a5, A1c+1A5b1+1B1b+1B2a6+1B2b5+2C1b, 1A2, 1A4, 1B1a+1B2a1+1B2a2+1B2a3+1B2a4+1B2c, 2+3, 4B+4C+4D+4F, 6 and 7A in Europa
Anth. non-traffic ROW	emissions of IPCCs sectors 1A1a, 1A1b+1B2a5, 1A1c+1A5b1+1B1b+1B2a6+1B2b5+2C1b, 1A2, 1A4, 1B1a+1B2a1+1B2a2+1B2a3+1B2a4+1B2c, 2+3, 4B+4C+4D+4F, 6 and 7A in rest of the world
Landtransport EU	emissions of IPCCs sectors 1A3b + 1A3c+1A3e in Europe
Landtransport ROW	emissions of IPCCs sectors 1A3b + 1A3c+1A3e in Rest of the World

S12.7 References

Grewe, V., Tsati, E., Mertens, M., Frömming, C., and Jöckel, P.: Contribution of emissions to concentrations: the TAGGING 1.0 submodel based on the Modular Earth Submodel System (MESSy 2.52), Geosci. Model Dev., 10, 2615–2633, doi:10.5194/gmd-10-2615-2017,https://www.geosci-model-dev.net/10/2615/2017/, 2017.

Guenther, A., Hewitt, C., E., D., Fall, R. G., C., Graedel, T., Harley, P., Klinger, L., Lerdau, M., McKay, W., Pierce, T., S., B., Steinbrecher, R., Tallamraju, R., Taylor, J., and Zimmermann, P.: A global model of natural volatile organic compound emissions, J. Geophys. Res., 100, 8873–8892, 1995.

Hofmann, C., Kerkweg, A., Wernli, H., and Jöckel, P.: The 1-way on-line coupled atmospheric chemistry model system MECO(n) Part 3: Meteorological evaluation of the on-line coupled system, Geosci. Model Dev., 5, 129–147, doi:10.5194/gmd-5-129-2012, http://www.geosci-model-dev.net/5/129/2012/, 2012.

Jöckel, P., Tost, H., Pozzer, A., Kunze, M., Kirner, O., Brenninkmeijer, C. A. M., Brinkop, S.,Cai, D. S., Dyroff, C., Eckstein, J., Frank, F., Garny, H., Gottschaldt, K.-D., Graf, P., Grewe,V., Kerkweg, A., Kern, B., Matthes, S., Mertens, M., Meul, S., Neumaier, M., Nützel, M.,Oberländer-Hayn, S., Ruhnke, R., Runde, T., Sander, R., Scharffe, D., and Zahn, A.: EarthSystem Chemistry integrated Modelling (ESCiMo) with the Modular Earth Submodel System(MESSy) version 2.51, Geosci. Model Dev., 9, 1153–1200, doi:10.5194/gmd-9-1153-2016, http://www.geosci-model-dev.net/9/ 1153/2016 /, 2016.

Kerkweg, A. and Jöckel, P.: The 1-way on-line coupled atmospheric chemistry model system MECO(n) Part 1: Description of the limited-area atmospheric chemistry model COSMO/MESSy, Geosci. Model Dev., 5, 87–110, doi:10.5194/gmd-5-87-2012, http://www.geosci-model-dev.net/5/87/2012/, 2012a.

Kerkweg, A. and Jöckel, P.: The 1-way on-line coupled atmospheric chemistry model system MECO(n) - Part 2: On-line coupling with the Multi-Model-Driver (MMD), Geosci. Model Dev., 5, 111–128, doi:10.5194/gmd-5-111-2012, http://www.geosci-model-dev.net/5/111/2012/, 2012b.

Pöschl, U., von Kuhlmann, R., Poisson, N., and Crutzen, P.: Development and Intercomparison of Condensed Isoprene Oxidation Mechanisms for Global Atmospheric Modeling, J. Atmos. Chem., 37, 29–152,doi:10.1023/A:1006391009798, 2000.

Price, C. and Rind, D.: Modeling Global Lightning Distributions in a General Circulation Model, Mon. Wea. Rev., 122, 1930–1939, doi:10.1175/1520-0493(1994)122h1930:MGLDIAi2.0.CO;2, doi.org/10.1175/1520-0493(1994)122<1930:MGLDIA>2.0.CO;2, 1994.

Rieger, V. S., Mertens, M., & Grewe, V.: An advanced method of contributing emissions to short-lived chemical species (OH and HO2): the TAGGING 1.1 submodel based on the Modular Earth Submodel System (MESSy 2.53), Geoscientific Model Development, 11, 2049–2066, doi: 10.5194/gmd-11-2049-2018, URL https://www.geosci-model-dev.net/11/2049/2018/. 2018

Wesely, M.: Parameterization of surface resistances to gaseous dry deposition in regional-scale numerical models, Atmospheric Environment (1967), 23, 1293–1304, doi: http://dx.doi.org/10.1016/0004-6981(89) 90153-4, http://www.sciencedirect.com/ science /article/pii/ 0004698189901534, 1989.

Yienger, J. J. and Levy, H.: Empirical model of global soil-biogenic NOx emissions, J. Geophys. Res. Atmos., 100, 11 447–11 464, doi:10.1029/95JD00370, URL http://dx.doi.org/10.1029/95JD00370, 1995.